

Supplemental Material for

“Correlators exceeding 1 in continuous measurements of superconducting qubits”

I. EXPERIMENTAL DETAILS

A. Setup and parameters

We have performed continuous quantum measurement of the qubit observable σ_z using the typical circuit QED setup, illustrated in Fig. 1 of the main text, generally similar to Ref. [S1] (though with important modifications). We use a 3D microwave cavity whose fundamental mode is dispersively coupled to a transmon qubit. The weakly-coupled input port is used to inject the Rabi drive and the readout tone. The stronger-coupled output port is used for the outgoing field. An additional cancellation tone (injected through circulator) displaces the outgoing field close to the vacuum, thus preventing saturation of the amplifier (the saturation becomes a serious problem for large angles φ_a).

The cavity frequency is 6.66 GHz and the qubit frequency is 4.26 GHz (the same as in Refs. [S2, S3]). The cavity mode decays with the rate $\kappa/2\pi = 7.2$ MHz, the qubit relaxation times are $T_1 = 60 \mu\text{s}$ and $T_2^* = 30 \mu\text{s}$. For qubit measurement, the cavity is coherently driven, causing the measurement-induced ensemble dephasing, which greatly exceeds intrinsic qubit dephasing. The resulting ensemble dephasing rate is $\Gamma = 1/1.8 \mu\text{s} = 2\pi \times 88$ kHz (for the results presented below in Sec. ID, $\Gamma = 1/1.6 \mu\text{s}$). The amplifier half-bandwidth is $B_{\text{amp}}/2\pi \simeq 10$ MHz. The detection quantum efficiency is $\eta = 0.44$.

For measurement of correlators, the qubit is prepared in the states $x_0 = \pm 1$, and then we apply the Rabi rotation about x -axis with frequency $\Omega_R/2\pi = \pm 1$ MHz (there are four combinations). The output signals from the continuous measurement are recorded for the duration of $4.88 \mu\text{s}$ with a timestep of 4 ns; after an additional averaging, the timestep is increased to $\Delta t = 40$ ns. We use only the traces, selected by heralding the ground state of the qubit at the start of a run and checking that the transmon qubit is still within the two-level subspace after the run [S3] (this eliminates about 25% of traces).

Experimental parameters satisfy the relation $\Gamma \ll |\Omega_r| \ll \kappa \lesssim B_{\text{amp}}$. This justifies the white noise and the “bad cavity” assumptions needed for the quantum Bayesian formalism [S4, S5]. Since $1/2T_1\Gamma = 0.015 \ll 1$, we can neglect energy relaxation in the analysis.

B. Calibration of response

The response $\Delta I(\varphi_a)$ is calibrated for each angle φ_a between the amplified quadrature and the informational (maximum response) quadrature. For this calibration, the qubit is initialized in the state $|1\rangle$ ($z_{\text{in}} = 1$) or $|0\rangle$

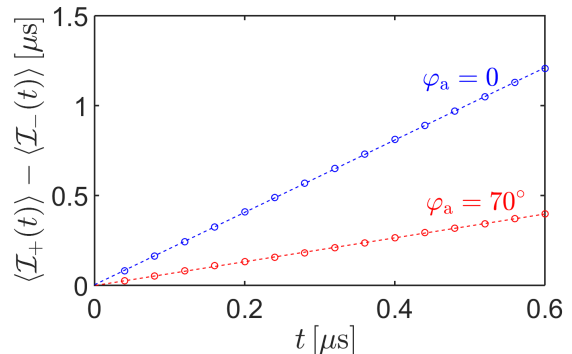


FIG. S1. Calibration of the detector response $\Delta I(\varphi_a)$ for $\varphi_a = 0$ and 70° . Detector response is obtained as the slope of the linear fit (dashed lines) to experimental results for $\langle \mathcal{I}_+(t) \rangle - \langle \mathcal{I}_-(t) \rangle$, depicted by circles. We find $\Delta I(0) = 2.01$ and $\Delta I(70^\circ) = 0.66$.

($z_{\text{in}} = -1$) and then continuously measured with no Rabi oscillations applied. For each initial state, we collect about 17,000 traces of the continuous (digitized with Δt) output signal $\tilde{I}(t)$, each of $4 \mu\text{s}$ duration. Units of $\tilde{I}(t)$ are arbitrary, but always the same (same gain of the amplifier).

To find the response $\Delta I(\varphi_a)$, for each trace we numerically calculate the integral

$$\mathcal{I}_\pm(t) = \int_0^t \tilde{I}_\pm(t') dt', \quad (\text{S1})$$

where the subscript \pm corresponds to initial state $z_{\text{in}} = \pm 1$, and then average over the ensemble of traces to get $\langle \mathcal{I}_\pm(t) \rangle$. The difference $\langle \mathcal{I}_+(t) \rangle - \langle \mathcal{I}_-(t) \rangle$ for $\varphi_a = 0$ and $\varphi_a = 70^\circ$ is shown in Fig. S1. From the slope of these practically straight lines, we find the response $\Delta I(\varphi_a) = d[\langle \mathcal{I}_+(t) \rangle - \langle \mathcal{I}_-(t) \rangle]/dt$. Note that we use only initial $0.6 \mu\text{s}$ of the process, because for a significantly longer integration there is a noticeable deviation from straight lines due to energy relaxation. From the slopes of lines in Fig. S1, we obtain the responses $\Delta I(0) = \Delta I_{\text{max}} = 2.01$ and $\Delta I(70^\circ) = 0.66$. This confirms the expected relation $\Delta I(\varphi_a) = \Delta I_{\text{max}} \cos \varphi_a$ within 3% inaccuracy.

To find the quantum efficiency η (even though we do not actually need it for the correlators), we first obtain the “measurement time” τ_m as $\tau_m(\varphi_a) = [2/\Delta I(\varphi_a)]^2 \times d\sigma^2(t)/dt$, where the variance $\sigma^2(t) = \sigma_\pm^2(t) \equiv \langle \mathcal{I}_\pm^2(t) \rangle - \langle \mathcal{I}_\pm(t) \rangle^2$ should theoretically be independent of φ_a and z_{in} . Figure S2 shows that indeed $\sigma_+^2(t) \approx \sigma_-^2(t)$, and they are almost the same for $\varphi_a = 0$ and $\varphi_a = 70^\circ$, so we practically have one straight line. From the linear fit, $d\sigma^2(t)/dt = 2.06 \mu\text{s}$, we obtain $\tau_m(0) = \tau_{\text{min}} \approx 2.04 \mu\text{s}$ and $\tau_m(70^\circ) = 18.9 \mu\text{s}$. Therefore, the quantum efficiency is $\eta = (2\Gamma\tau_{\text{min}})^{-1} = 0.44$.

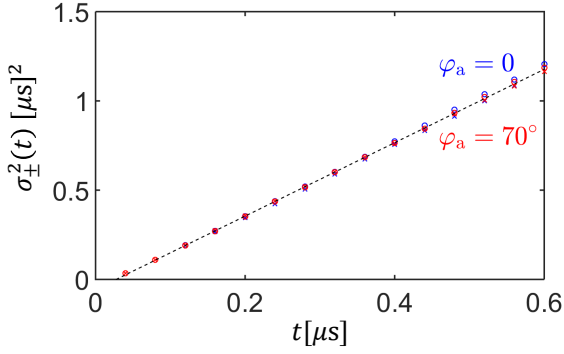


FIG. S2. The variance $\sigma_{\pm}^2(t) \equiv \langle \mathcal{I}_{\pm}^2(t) \rangle - \langle \mathcal{I}_{\pm}(t) \rangle^2$ as a function of the integration time t . Circles show σ_+ , crosses show σ_- , blue symbols are for $\varphi_a = 0$, red symbols are for $\varphi_a = 70^\circ$. All four cases can be fitted by one straight (dashed) line with slope $d\sigma^2(t)/dt = 2.06 \mu\text{s}$, which gives $\tau_m(0) = 2.04 \mu\text{s}$ and $\tau_m(70^\circ) = 18.9 \mu\text{s}$.

C. Correlators

For measurement of correlators, the qubit is prepared at time $t_0 = 0$ in the pure state $\mathbf{r}_0 = (\pm 1, 0, 0)$ and then is Rabi-rotated about x -axis with frequency $\Omega_R/2\pi = \pm 1$ MHz (four combinations), while being continuously measured along z -axis. The ensemble-averaged evolution is supposed to change (decrease) only x component of the qubit state, while z and y components should remain zero on average. We obtain experimental correlators as

$$K(\tau) = \frac{1}{T} \int_{t_{\text{skip}}}^{t_{\text{skip}}+T} \left\langle \frac{\tilde{I}(t_1) - \langle \tilde{I}(t_1) \rangle}{\Delta I(\varphi_a)} \times \frac{\tilde{I}(t_1 + \tau) - \langle \tilde{I}(t_1 + \tau) \rangle}{\Delta I(\varphi_a)} \right\rangle dt_1, \quad (\text{S2})$$

where the averaging time is $T = 0.28 \mu\text{s}$ (to reduce fluctuations) and the discarded initial duration is $t_{\text{skip}} = 0.28 \mu\text{s}$ (to avoid initial transients in the data). Note that both T and t_{skip} are small in comparison with $1/\Gamma = 1.8 \mu\text{s}$ and duration of $4.88 \mu\text{s}$ of the recorded traces.

Since on average $z(t) = 0$ for $x_0 = \pm 1$ and Rabi rotation over x -axis, the average $\langle \tilde{I}(t) \rangle$ in Eq. (S2) should theoretically be a constant offset \tilde{I}_0 . However, this is not exactly the case in the experiment, as seen from Fig. S3, which shows $\langle \tilde{I}(t) \rangle$ for all four combinations of x_0 and Ω_R in the case $\varphi_a = 70^\circ$. Besides the overall shift, $\tilde{I}_0 \simeq -0.4$, we see small periodic features, the reason for which is unclear. Note that the size of these features ($\simeq \pm 0.1$) is small in comparison with the response (0.66) and noise in an individual trace ($\sigma_{\Delta t} \approx 6$); however, they still slightly affect the correlators. This is why we subtract $\langle \tilde{I}(t) \rangle$ in Eq. (S2) instead of subtracting a constant offset \tilde{I}_0 , in order to remove the fluctuating offsets. Moreover, we calculate $\langle \tilde{I}(t) \rangle$ in Eq. (S2) by averaging over a relatively small number of neighboring runs (about 3,000), in order

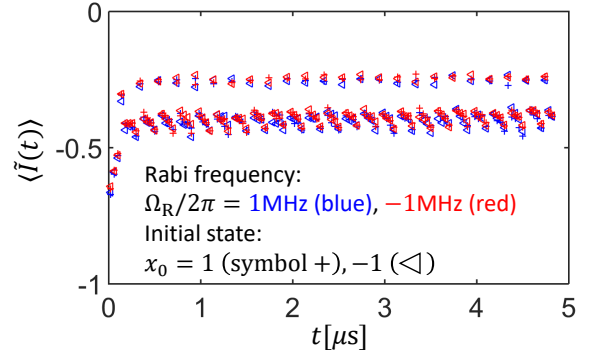


FIG. S3. The offset $\langle \tilde{I}(t) \rangle$ for the initial state $x_0 = 1$ (crosses) or $x_0 = -1$ (triangles) and Rabi frequency $\Omega_R = 1$ MHz (blue symbols) or -1 MHz (red symbols). The data points are separated by $\Delta t = 40$ ns.

to account for offsets, slowly fluctuating in time. Figure S3 also explains why we use $t_{\text{skip}} = 0.28 \mu\text{s}$, i.e., skip first seven data points, for which some transient process is easily noticeable.

To calculate the theoretical result for the two-time correlator, we use Eq. (20) of the main text with $\mathbf{r}(t_1 - 0) = (e^{-\Gamma t_1} x_0, 0, 0)$. Solving the ensemble-averaged qubit evolution (energy relaxation is neglected), we obtain the correlator

$$K(t_1, t_1 + \tau) = \left[\cos(\tilde{\Omega}_R \tau) + \frac{\Gamma}{2\tilde{\Omega}_R} \sin(\tilde{\Omega}_R \tau) \right] e^{-\Gamma\tau/2} + x_0 e^{-\Gamma t_1} \frac{\tan \varphi_a \Omega_R}{\tilde{\Omega}_R} \sin(\tilde{\Omega}_R \tau) e^{-\Gamma\tau/2}, \quad (\text{S3})$$

where $\tilde{\Omega}_R = \sqrt{\Omega_R^2 - \Gamma^2/4}$. To perform the additional integration over t_1 in Eq. (S2), we notice that t_1 enters Eq. (S3) only via the factor $e^{-\Gamma t_1}$ in the second term. Therefore, the only change in Eq. (S3) is the replacement

$$x_0 \rightarrow c x_0, \quad c = e^{-\Gamma t_{\text{skip}}} \frac{1 - e^{-\Gamma T}}{\Gamma T}. \quad (\text{S4})$$

Thus we obtain Eq. (23) of the main text,

$$K(\tau) = \left[\cos(\tilde{\Omega}_R \tau) + \frac{\Gamma}{2\tilde{\Omega}_R} \sin(\tilde{\Omega}_R \tau) \right] e^{-\Gamma\tau/2} + c x_0 \tan \varphi_a \frac{\Omega_R}{\tilde{\Omega}_R} \sin(\tilde{\Omega}_R \tau) e^{-\Gamma\tau/2}. \quad (\text{S5})$$

Figure S4 shows experimental results (symbols) and analytics (lines) for the correlators $K(\tau)$ for $\varphi_a = 70^\circ$ in the four cases: for Rabi frequency $\Omega_R/2\pi = 1$ MHz (upper panel) or -1 MHz (lower panel) and initial state $x_0 = 1$ (blue circles and blue lines) or $x_0 = -1$ (red crosses and red lines). There is a good agreement between the theory and experiment in all the four cases. In Fig. 3(a) of the main text we present the same results, additionally averaged over two cases with the same product $\Omega_R x_0$.

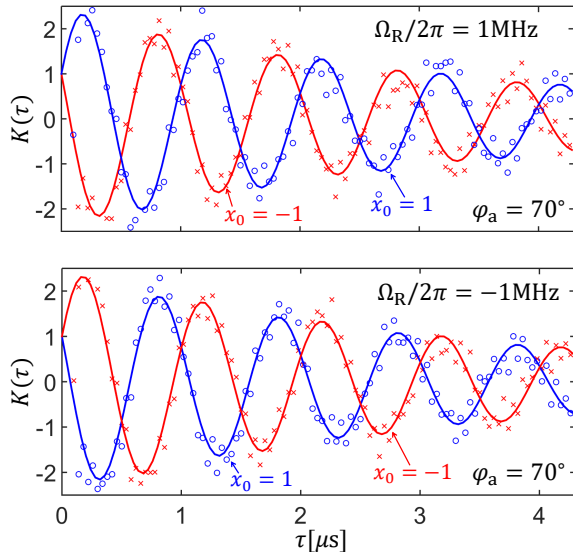


FIG. S4. Experimental correlators (symbols) and analytics (lines) for the four cases with $\Omega_R/2\pi = \pm 1$ MHz and $x_0 = \pm 1$. The amplified-quadrature angle determining the phase backaction is $\varphi_a = 70^\circ$, time-averaging parameters are $T = 0.28 \mu\text{s}$ and $t_{\text{skip}} = 0.28 \mu\text{s}$, ensemble averaging is over 3.2×10^5 traces in each case.

D. Correlators for other angles φ_a

We have also measured the correlators for angles $\varphi_a = 0, 40^\circ$, and 80° . This was done on a different date compared with the results presented in Sections IB, IC, and in the main text, so parameters are slightly different. In particular, the qubit ensemble dephasing rate during measurement is $\Gamma = 1/1.6 \mu\text{s}$ (a slightly higher microwave power for measurement). The detector responses are $\Delta I(0) = 2.3$, $\Delta I(40^\circ) = 1.75$, and $\Delta I(80^\circ) = 0.44$. The relation $\Delta I(\varphi_a) = \Delta I_{\text{max}} \cos(\varphi_a)$ is satisfied with 1% inaccuracy for 40° and with 10% inaccuracy for 80° (inaccuracy grows with decrease of the SNR).

Figure S5 shows the experimental correlators (symbols) and theoretical results (lines) for the angles $\varphi_a = 0, 40^\circ$ and 80° . We use $\Omega_R/2\pi = 1$ MHz (only one direction) and $x_0 = \pm 1$, the time-integration parameters are still $T = t_{\text{skip}} = 0.28 \mu\text{s}$. The experimental correlators for $\varphi_a = 0$ agree with the theory very well; they are practically the same for $x_0 = 1$ and $x_0 = -1$ (theoretically there is no dependence on the initial state [S3]), and $|K(\tau)| \leq 1$ always because there is no phase backaction. Experimental correlators for $\varphi_a = 40^\circ$ also agree well with the theory; the correlator $K(\tau)$ for $x_0 = 1$ marginally exceeds 1 at only one point. Experimental correlators for $\varphi_a = 80^\circ$ greatly exceed 1 at many points, reaching values up to $K_{\text{max}} \simeq 5$. However, there is a significant deviation from the theory, which is somewhat expected since the SNR greatly decreases for angles φ_a close to $\pi/2$.

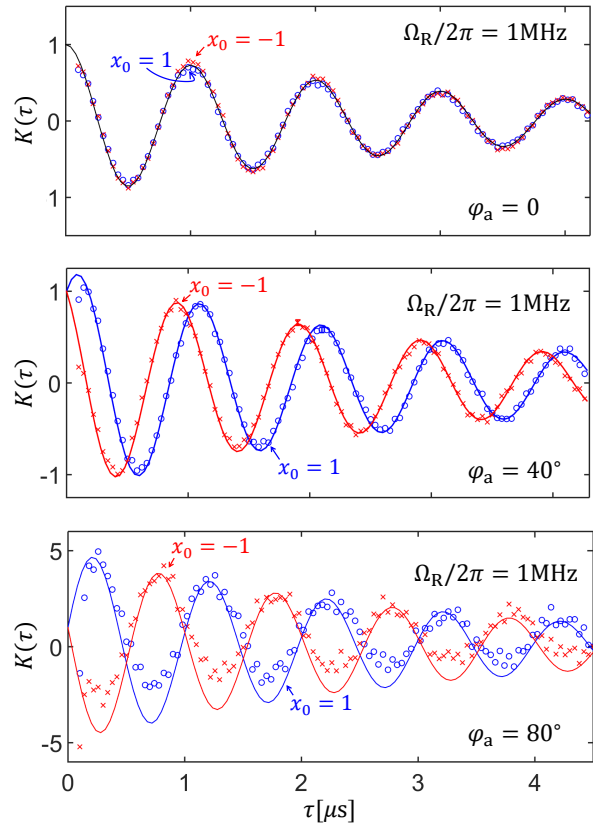


FIG. S5. Experimental correlators (symbols) and theoretical predictions (lines) for angles $\varphi_a = 0$ (top panel), 40° (middle panel), and 80° (bottom panel). Initial states are $x_0 = 1$ (blue circles and lines) and $x_0 = -1$ (red crosses and lines), Rabi frequency is $\Omega_R = 1$ MHz.

II. GENERALIZED COLLAPSE RECIPE FOR MULTI-TIME MULTI-DETECTOR CORRELATORS

In this section we prove the generalized collapse recipe (GCR) for multi-time correlators from simultaneous continuous measurement of N_d noncommuting qubit observables $\sigma_\ell = \mathbf{n}_\ell \sigma$, where \mathbf{n}_ℓ is the ℓ th measurement axis direction on the Bloch sphere and $\ell = 1, \dots, N_d$.

In this case, the quantum Bayesian equation for qubit evolution in Itô interpretation is [cf. Eq. (4) of the main text]

$$\dot{\mathbf{r}} = \Lambda_{\text{ens}}(\mathbf{r} - \mathbf{r}_{\text{st}}) + \sum_{\ell=1}^{N_d} \left[\frac{\mathbf{n}_\ell - (\mathbf{n}_\ell \mathbf{r}) \mathbf{r}}{\sqrt{\tau_\ell}} + \mathcal{K}_\ell \frac{(\mathbf{n}_\ell \times \mathbf{r})}{\sqrt{\tau_\ell}} \right] \xi_\ell(t), \quad (\text{S6})$$

where τ_ℓ is the “measurement time” for the ℓ th detector and $\mathcal{K}_\ell = \tan \varphi_\ell^a$ determines the corresponding relative strength of phase backaction. The normalized output signal from the ℓ th detector is modeled as

$$I_\ell(t) = \text{Tr}[\sigma_\ell \rho(t)] + \sqrt{\tau_\ell} \xi_\ell(t) = \mathbf{n}_\ell \mathbf{r}(t) + \sqrt{\tau_\ell} \xi_\ell(t), \quad (\text{S7})$$

where ξ_ℓ are uncorrelated white noises,

$$\langle \xi_\ell(t) \xi_{\ell'}(t') \rangle = \delta_{\ell\ell'} \delta(t-t'). \quad (\text{S8})$$

Let us consider the N -time correlator

$$K_{\ell_1 \dots \ell_N}(t_1, \dots, t_N) \equiv \langle I_{\ell_N}(t_N) \cdots I_{\ell_2}(t_2) I_{\ell_1}(t_1) \rangle, \quad (\text{S9})$$

in which the time arguments are ordered as $t_1 < t_2 < \dots < t_N$ and N can be smaller, equal, or larger than N_d . We will prove that this correlator can be obtained from the GCR formula

$$\begin{aligned} K_{\ell_1 \dots \ell_N}^{\text{GCR}}(t_1, \dots, t_N) \\ = \sum_{\{I_{\ell_j} = \pm 1\}}^{2^N} \left[\prod_{j=2}^{j=N} I_{\ell_j} p(I_{\ell_j}, t_j | I_{\ell_{j-1}}, t_{j-1}) \right] I_{\ell_1} p(I_{\ell_1}, t_1), \end{aligned} \quad (\text{S10})$$

where the sum is over 2^N scenarios of obtaining discrete outcomes $I_{\ell_j} = \pm 1$ of (fictitious) ‘‘strong’’ measurements at time moments t_j ($j = 1, \dots, N$),

$$p(I_{\ell_1}, t_1) = \frac{1 + I_{\ell_1} \mathbf{n}_{\ell_1} \mathbf{r}(t_1 - 0)}{2} \quad (\text{S11})$$

is the probability to get the first outcome $I_{\ell_1} = \pm 1$ at time t_1 , and

$$p(I_{\ell_j}, t_j | I_{\ell_{j-1}}, t_{j-1}) = \frac{1 + I_{\ell_j} \mathbf{n}_{\ell_j} \mathbf{r}_{\text{ens}}(t_j | I_{\ell_{j-1}} \mathbf{r}_{\text{coll}}^{(j-1)}, t_{j-1})}{2} \quad (\text{S12})$$

is the ‘‘conditional probability’’ to get the outcome I_{ℓ_j} at time t_j ($j \geq 2$) given that we got the outcome $I_{\ell_{j-1}}$ at time t_{j-1} (this ‘‘probability’’ can be negative or larger than 1). We assume (pretend) that the strong measurement of σ_{ℓ_j} (with phase backaction) at time t_j with the result $I_{\ell_j} = \pm 1$ collapses (abruptly moves) the qubit state to

$$\mathbf{r}(t_j + 0) = I_{\ell_j} \mathbf{r}_{\text{coll}}^{(j)} = I_{\ell_j} [\mathbf{n}_{\ell_j} + \mathcal{K}_{\ell_j} \mathbf{n}_{\ell_j} \times \mathbf{r}(t_j - 0)], \quad (\text{S13})$$

while at other times, $t \neq t_j$, the qubit evolution is given by the ensemble-averaged equation

$$\dot{\mathbf{r}}_{\text{ens}} = \Lambda_{\text{ens}}(\mathbf{r}_{\text{ens}} - \mathbf{r}_{\text{st}}). \quad (\text{S14})$$

Therefore, in each of the 2^N scenarios, we have a different sequence of after-collapse states $I_{\ell_j} \mathbf{r}_{\text{coll}}^{(j)}$, with

$$\mathbf{r}_{\text{coll}}^{(1)} = \mathbf{n}_{\ell_1} + \mathcal{K}_{\ell_1} \mathbf{n}_{\ell_1} \times \mathbf{r}(t_1 - 0) \quad (\text{S15})$$

for the first collapse, and then for $j \geq 2$ we have

$$\mathbf{r}_{\text{coll}}^{(j)} = \mathbf{n}_{\ell_j} + \mathcal{K}_{\ell_j} \mathbf{n}_{\ell_j} \times \mathbf{r}_{\text{ens}}(t_j | I_{\ell_{j-1}} \mathbf{r}_{\text{coll}}^{(j-1)}, t_{j-1}), \quad (\text{S16})$$

where $\mathbf{r}_{\text{ens}}(t | \mathbf{r}_{\text{in}}, t_{\text{in}})$ is the solution of Eq. (S14) with initial condition $\mathbf{r}_{\text{ens}}(t_{\text{in}} | \mathbf{r}_{\text{in}}, t_{\text{in}}) = \mathbf{r}_{\text{in}}$, and $\mathbf{r}(t_1 - 0) = \mathbf{r}_{\text{ens}}(t_1 | \mathbf{r}_0, t_0)$ if the procedure starts at time $t_0 < t_1$ with the initial state \mathbf{r}_0 .

Note that the initial qubit state should be physical, and therefore the 3-vector \mathbf{r}_0 should be within the Bloch sphere, $|\mathbf{r}_0| \leq 1$. However, after each collapse, the state $I_{\ell_j} \mathbf{r}_{\text{coll}}^{(j)}$ will be outside the Bloch sphere (if $\mathcal{K}_{\ell_j} \neq 0$). Therefore, the state before the next collapse may also be outside the Bloch sphere, and then the ‘‘conditional probabilities’’ for the next outcome $I_{\ell_{j+1}} = \pm 1$ may be negative or larger than 1 – see Eq. (S12). Also note that the 3×3 matrix Λ_{ens} in Eq. (S14) takes into account unitary evolution, continuous measurement by all N_d detectors, and possible additional decoherence. Both Λ_{ens} and \mathbf{r}_{st} can depend on time. The formal solution of Eq. (S14) can still be written in the same form as in the main text,

$$\mathbf{r}_{\text{ens}}(t | \mathbf{r}_{\text{in}}, t_{\text{in}}) = \mathcal{P}(t | t_{\text{in}}) \mathbf{r}_{\text{in}} + \mathcal{P}_{\text{st}}(t | t_{\text{in}}), \quad (\text{S17})$$

where $\mathcal{P}(t | t')$ is a 3×3 matrix satisfying equation $\partial_t \mathcal{P}(t | t') = \Lambda_{\text{ens}}(t) \mathcal{P}(t | t')$ with $\mathcal{P}(t' | t') = \mathbb{1}$, and $\mathcal{P}_{\text{st}}(t | t') = - \int_{t'}^t \mathcal{P}(t | t'') \Lambda_{\text{ens}}(t'') \mathbf{r}_{\text{st}}(t'') dt''$.

To prove that Eqs. (S10)–(S16) give the correct value for the multi-time correlator (S9), let us first carry out the summation over the last outcome I_{ℓ_N} in Eq. (S10) and represent the result as

$$K_{\ell_1 \dots \ell_N}^{\text{GCR}}(t_1, \dots, t_N) = \mathbf{n}_{\ell_N} \mathbf{K}_{\ell_1 \dots \ell_N}^{\text{GCR}}(t_1, \dots, t_N), \quad (\text{S18})$$

where we have introduced the vector-valued correlator

$$\begin{aligned} \mathbf{K}_{\ell_1 \dots \ell_N}^{\text{GCR}}(t_1, \dots, t_N) \equiv \sum_{\{I_{\ell_j} = \pm 1\}}^{2^{N-1}} \mathbf{r}_{\text{ens}}(t_N | I_{\ell_{N-1}} \mathbf{r}_{\text{coll}}^{(N-1)}, t_{N-1}) \\ \times \left[\prod_{j=2}^{j=N-1} I_{\ell_j} p(I_{\ell_j}, t_j | I_{\ell_{j-1}}, t_{j-1}) \right] I_{\ell_1} p(I_{\ell_1}, t_1). \end{aligned} \quad (\text{S19})$$

We then apply Eq. (S17) to Eq. (S19), use Eq. (S16) with $j = N - 1$ and use the relations (S9) and (S18)–(S19) to obtain the recursive formula

$$\begin{aligned} \mathbf{K}_N^{\text{GCR}} = \mathcal{P}(t_N | t_{N-1}) \left[\mathbf{n}_{\ell_{N-1}} \mathbf{K}_{N-2}^{\text{GCR}} \right. \\ \left. + \mathcal{K}_{\ell_{N-1}} \mathbf{n}_{\ell_{N-1}} \times \mathbf{K}_{N-1}^{\text{GCR}} \right] + \mathbf{K}_{N-1}^{\text{GCR}} \mathcal{P}_{\text{st}}(t_N | t_{N-1}), \end{aligned} \quad (\text{S20})$$

where for brevity $\mathbf{K}_N^{\text{GCR}} \equiv \mathbf{K}_{\ell_1 \dots \ell_N}^{\text{GCR}}(t_1, \dots, t_N)$ and $\mathbf{K}_N^{\text{GCR}} \equiv \mathbf{K}_{\ell_1 \dots \ell_N}^{\text{GCR}}(t_1, \dots, t_N)$. This recursion for N needs two initial cases, for which $N = 2$ and $N = 1$ can be used. The correlators for $N = 1$ are trivial,

$$\mathbf{K}_{\ell_1}^{\text{GCR}}(t_1) = \mathbf{r}(t_1 - 0) \quad (\text{S21})$$

and therefore $\mathbf{K}_{\ell_1}^{\text{GCR}}(t_1) = \mathbf{n}_{\ell_1} \mathbf{r}(t_1 - 0)$, while the GCR correlators for $N = 2$ are [cf. Eq. (10) of the main text]

$$\begin{aligned} \mathbf{K}_{\ell_1 \ell_2}^{\text{GCR}}(t_1, t_2) = \mathbf{r}_{\text{ens}}(t_2 | \mathbf{r}_{\text{coll}}^{(1)}, t_1) \frac{1 + \mathbf{n}_{\ell_1} \mathbf{r}(t_1 - 0)}{2} \\ - \mathbf{r}_{\text{ens}}(t_2 | -\mathbf{r}_{\text{coll}}^{(1)}, t_1) \frac{1 - \mathbf{n}_{\ell_1} \mathbf{r}(t_1 - 0)}{2} \end{aligned} \quad (\text{S22})$$

and correspondingly $K_{\ell_1 \ell_2}^{\text{GCR}}(t_1, t_2) = \mathbf{n}_{\ell_2} \mathbf{K}_{\ell_1 \ell_2}^{\text{GCR}}(t_1, t_2)$. Using Eq. (S17), it is easy to see that Eq. (S22) can be obtained from the recursion (S20) if we formally define

$$K_0^{\text{GCR}} = 1. \quad (\text{S23})$$

Thus far, we have just rewritten the GCR in a recursive form [Eqs. (S18) and (S20)]. Next, we will show that the same recursive relations for the correlators [including the initial cases (S21)–(S23)] can be obtained from the quantum Bayesian equations Eq. (S6)–(S7), thus proving the GCR.

Now we are considering the actual process (not the fictitious scenarios of the GCR), so $I_\ell(t)$ are continuous noisy signals – see Eq. (S7). Using the causality property $\langle \xi_\ell(t) I_{\ell'}(t') \rangle = 0$ for $t > t'$, we can express the multi-time correlator (S9) in the same form as Eq. (S18),

$$K_{\ell_1 \dots \ell_N}(t_1, \dots, t_N) = \mathbf{n}_{\ell_N} \mathbf{K}_{\ell_1 \dots \ell_N}(t_1, \dots, t_N), \quad (\text{S24})$$

where we have introduced the vector-valued correlator

$$\mathbf{K}_{\ell_1 \dots \ell_N}(t_1, \dots, t_N) \equiv \langle \mathbf{r}_N I_{\ell_{N-1}}(t_{N-1}) \dots I_{\ell_1}(t_1) \rangle \quad (\text{S25})$$

and for brevity we use notation $\mathbf{r}_N \equiv \mathbf{r}(t_N)$. Also introducing the short notation $\mathbf{K}_N \equiv \mathbf{K}_{\ell_1 \dots \ell_N}(t_1, \dots, t_N)$ and using Eq. (S7) for $I_{\ell_{N-1}}(t)$, we can write \mathbf{K}_N as a sum of two terms,

$$\mathbf{K}_N = \mathbf{K}_N^{(1)} + \mathbf{K}_N^{(2)}, \quad (\text{S26a})$$

$$\mathbf{K}_N^{(1)} \equiv \langle \mathbf{r}_N (\mathbf{n}_{\ell_{N-1}} \mathbf{r}_{N-1}) I_{\ell_{N-2}}(t_{N-2}) \dots I_{\ell_1}(t_1) \rangle, \quad (\text{S26b})$$

$$\mathbf{K}_N^{(2)} \equiv \langle \mathbf{r}_N \sqrt{\tau_{\ell_{N-1}}} \xi_{\ell_{N-1}}(t_{N-1}) I_{\ell_{N-2}}(t_{N-2}) \dots I_{\ell_1}(t_1) \rangle. \quad (\text{S26c})$$

We now consider $\mathbf{K}_N^{(1)}$ and $\mathbf{K}_N^{(2)}$ as functions of t_N . By differentiating them over t_N and using Eq. (S6), we obtain the following equations of motion

$$\partial_{t_N} \mathbf{K}_N^{(1)} = \Lambda_{\text{ens}} \left[\mathbf{K}_N^{(1)} - \mathbf{r}_{\text{st}} K_{N-1} \right], \quad (\text{S27a})$$

$$\partial_{t_N} \mathbf{K}_N^{(2)} = \Lambda_{\text{ens}} \mathbf{K}_N^{(2)}. \quad (\text{S27b})$$

The initial condition for $\mathbf{K}_N^{(1)}$ is

$$\begin{aligned} \mathbf{K}_N^{(1)}(t_{N-1}) &\equiv \mathbf{K}_{\ell_1 \dots \ell_N}^{(1)}(t_N = t_{N-1}, t_{N-1}, \dots, t_1) \\ &= \langle \mathbf{r}_{N-1} (\mathbf{n}_{\ell_{N-1}} \mathbf{r}_{N-1}) I_{\ell_{N-2}}(t_{N-2}) \dots I_{\ell_1}(t_1) \rangle, \end{aligned} \quad (\text{S28})$$

and the initial condition for $\mathbf{K}_N^{(2)}$ can be obtained by averaging over the noise $\xi_{\ell_{N-1}}(t_{N-1})$ in the same way as in the main text (for the two-time correlator), that gives

$$\begin{aligned} \mathbf{K}_N^{(2)}(t_{N-1}) &\equiv \mathbf{K}_{\ell_1 \dots \ell_N}^{(2)}(t_N = t_{N-1}, t_{N-1}, \dots, t_1) = \\ &\langle [\mathbf{n}_{\ell_{N-1}} - (\mathbf{n}_{\ell_{N-1}} \mathbf{r}_{N-1}) \mathbf{r}_{N-1} + \mathcal{K}_{\ell_{N-1}} (\mathbf{n}_{\ell_{N-1}} \times \mathbf{r}_{N-1})] \\ &\quad \times I_{\ell_{N-2}}(t_{N-2}) \dots I_{\ell_1}(t_1) \rangle. \end{aligned} \quad (\text{S29})$$

We then solve the linear equations (S27) using (S17),

$$\mathbf{K}_N^{(1)} = \mathcal{P}(t_N | t_{N-1}) \mathbf{K}_N^{(1)}(t_{N-1}) + \mathcal{P}_{\text{st}} K_{N-1}, \quad (\text{S30a})$$

$$\mathbf{K}_N^{(2)} = \mathcal{P}(t_N | t_{N-1}) \mathbf{K}_N^{(2)}(t_{N-1}), \quad (\text{S30b})$$

and inserting the initial conditions (S28)–(S29), we find

$$\begin{aligned} \mathbf{K}_N^{(1)} + \mathbf{K}_N^{(2)} &= \mathcal{P}(t_N | t_{N-1}) \times \\ &\langle [\mathbf{n}_{\ell_{N-1}} + \mathcal{K}_{\ell_{N-1}} (\mathbf{n}_{\ell_{N-1}} \times \mathbf{r}_{N-1})] I_{\ell_{N-2}}(t_{N-2}) \dots I_{\ell_1}(t_1) \rangle \\ &+ \mathcal{P}_{\text{st}}(t_N | t_{N-1}) K_{N-1}, \end{aligned} \quad (\text{S31})$$

where K_N is the short notation for the correlator (S24).

Finally, using Eqs. (S9), (S25), and (S26a), the result (S31) can be rewritten as a recursion,

$$\begin{aligned} \mathbf{K}_N &= \mathcal{P}(t_N | t_{N-1}) [\mathbf{n}_{\ell_{N-1}} K_{N-2} \\ &+ \mathcal{K}_{\ell_{N-1}} (\mathbf{n}_{\ell_{N-1}} \times \mathbf{K}_{N-1})] + \mathcal{P}_{\text{st}}(t_N | t_{N-1}) K_{N-1}, \end{aligned} \quad (\text{S32})$$

which is exactly the same as Eq. (S20) for the vector-valued correlators obtained via the GCR method [recall that Eq. (S24) is also the same as Eq. (S18)]. It is easy to see that \mathbf{K}_N in the initial cases $N = 1$ and $N = 2$ for the recursive relation (S32) also coincide with the results (S21) and (S22) for the GCR method [so that we can still define $K_0 = 1$ as in Eq. (S23)]. This proves that $\mathbf{K}_N = \mathbf{K}_N^{\text{GCR}}$, so any multi-time multi-detector correlator calculated via the generalized collapse recipe coincides with the correlator given by the quantum Bayesian formalism. The obvious advantage of the recipe is simplicity of calculations compared with the direct quantum Bayesian simulations.

Note that for a single detector ($N_d = 1$), the correlators can be larger than 1 only in the presence of a unitary evolution. This is because the projection of the collapsed state (S13) on the measurement axis is ± 1 (even though it is outside the Bloch sphere), and without unitary evolution (only decoherence) this projection remains within the ± 1 range. In contrast, for detectors of non-commuting observables, the correlators can exceed 1 even without unitary evolution, only due to phase backaction. As an example, for continuous measurement of σ_z and σ_x [S2], the two-time cross-correlator $K_{zx}(t_1, t_2)$ exceeds 1 for small positive values of t_1 and $t_2 - t_1$ if the initial state is $\mathbf{r}(0) = (0, -1, 0)$ and the phase backaction for σ_z -measurement is sufficiently strong, $\mathcal{K}_z = \tan \varphi_z^a > 1$. A weaker phase backaction would also produce cross-correlator larger than 1 if σ_x measurement is replaced with the measurement along the direction between x and z .

We emphasize that the GCR is only a recipe to obtain correct values of the correlators from continuous measurement of a qubit. For actual evolution of the qubit, the quantum Bayesian/trajectory equation (S6) should be used. It is in principle possible to obtain correlators from the actual evolution (e.g., using Monte Carlo simulations). However, obtaining the same values for the correlators is much simpler using the GCR. The GCR uses a

fictitious evolution: in particular, actual continuous measurements are replaced with “strong” measurements at time moments t_j , which may produce unphysical states

outside the Bloch sphere. Nevertheless, the correlators obtained from this fictitious evolution coincide with actual correlators.

-
- [S1] K. W. Murch, S. J. Weber, C. Macklin, and I. Siddiqi, *Nature* **502**, 211 (2013).
[S2] S. Hacoheh-Gourgy, L. S. Martin, E. Flurin, V. V. Ramasesh, K. B. Whaley, and I. Siddiqi, *Nature* **538**, 491

- (2016).
[S3] J. Atalaya, S. Hacoheh-Gourgy, L. S. Martin, I. Siddiqi, and A. N. Korotkov, *npj Quantum Inf.* **4**, 41 (2018).
[S4] A. N. Korotkov, arXiv:1111.4016.
[S5] A. N. Korotkov, *Phys. Rev. A* **94**, 042326 (2016).